The dsRBP Staufen2 governs RNP assembly of neuronal Argonaute proteins

Janina Ehses [1], Melina Schlegel[1], Luise Schröger [1], Rico Schieweck[1], Sophia Derdak [2], Martin Bilban[3], Karl Bauer[1], Max Harner[1] and Michael A. Kiebler [1,*]

[1]Biomedical Center (BMC), Department for Cell Biology, Medical Faculty, Ludwig-Maximilians-University of Munich, 82152 Planegg-Martinsried, Germany, [2]Core Facilities, Medical University of Vienna, 1090 Vienna, Austria and [3]Department of Laboratory Medicine and Core Facility Genomics, Medical University, of Vienna, 1090 Vienna, Austria

ABSTRACT

Mature microRNAs are bound by a member of the Argonaute (Ago1-4) protein family, forming the core of the RNA-induced silencing complex (RISC). Association of RISC with target mRNAs results in ribonucleoprotein (RNP) assembly involved in translational silencing or RNA degradation. Yet, the dynamics of RNP assembly and its underlying functional implications are unknown. Here, we have characterized the role of the RNA-binding protein Staufen2, a candidate Ago interactor, in RNP assembly. Staufen2 depletion resulted in the upregulation of Ago1/2 and the RISC effector proteins Ddx6 and Dcp1a. This upregulation was accompanied by the displacement of Ago1/2 from processing bodies, large RNPs implicated in RNA storage, and subsequent association of Ago2 with polysomes. In parallel, Staufen2 deficiency decreased global translation and increased dendritic branching. As the observed phenotypes can be rescued by Ago1/2 knockdown, we propose a working model in which both Staufen2 and Ago proteins depend on each other and contribute to neuronal homeostasis.

INTRODUCTION

Posttranscriptional gene regulation is an important cellular mechanism, which is mediated through a network of thousands of RNA-binding proteins (RBPs) (1–3). It is the RNA that serves as platform for the combinatorial assembly of different RBPs. Their intertwined action actually determines the fate of the RNA (1,4). The association of RNAs and proteins results in the formation of RNA granules, often termed ribonucleoprotein particles (RNPs), that show large heterogeneity in composition, size and function (5,6). Depending on the composition and condensation grade of

RNA and protein components within the particles, the dynamic of RNP assembly differs (7,8). While transport RNPs have been shown to contain only few transcripts and mediate RNA localization and local translation (5,9,10), larger assemblies such as stress granules or cytosolic processing bodies (P-bodies) are thought to rather serve in RNA and RBP storage (5,6,11).

Specific RNA structures rather than primary binding sequences are preferentially recognized by double-stranded RBPs (dsRBPs), thereby regulating RNA condensation grade and RNA accessibility for other RBPs. The neuron-enriched Staufen2 (Stau2) protein is a dsRBP that preferentially binds to the 3′-UTR of target RNAs (12) and, as a part of transport RNPs, enables their directed dendritic transport (13,14). Stau2 regulates activity-dependent dendritic mRNA localization (12) and is required for maintenance of general dendritic RNA content (15). A large subset of Stau2 targets encodes for synaptic proteins, with a prominent enrichment of members acting in the G protein-coupled receptor pathway (16). Finally, *in vivo* and *in vitro* studies have shown that defective or missing Stau2 yield abnormal dendritic spines (17) and deficits in long-term depression (18,19). On the protein level, Stau2 is known to interact with several other RBPs, including some involved in RNA interference (RNAi) and translation repression, mainly in an RNA-dependent manner (20). One core component of the RNAi machinery is the ubiquitously expressed RBP belonging to the Argonaute protein family (Ago1–4). For RNAi, small RNAs, such as microRNAs (miRNAs), are transcribed, processed and loaded onto Ago, where they serve as a guide strand to recognize a set of target mRNAs (21,22). This RNA induced silencing complex (RISC) then leads to translation repression and/or RNA degradation of the target mRNA. On the mechanistic level, this is achieved by recruitment of downstream effector proteins such as GW182/Tnrc6, Ddx6 and CCR4-NOT (23). In addition, direct RNA degradation can be achieved by the intrinsic slicer activity of Ago2 (24). The importance of Ago2 and RISC is highlighted by the findings that loss of Ago2 in

mice leads to embryonic lethality and Ago2 germline mutants to central nervous system abnormalities in humans (24,25). Both Ago and RISC effector proteins are enriched in P-bodies (11), but also exist in the cytosol. Certain members, such as Ago2, Dicer or TRBP, even localize to distal dendrites, where they exert neuronal activity dependent functions (26,27).

Individual RNAi components have been shown to exist in neuronal Stau2 RNPs (20,28). Here, we aimed to unravel the underlying network of Stau2 and RBPs involved in RNAi. The synergistic or antagonistic mechanisms between different RBPs have been extensively studied on the single target level (29). Cellular RNP remodeling, however, upon alteration of single RBPs has rarely been looked at so far. We provide experimental evidence that the neuronal RBP Stau2 regulates key RISC protein expression, while global miRNA abundance appears unaffected by Stau2. Further, Stau2 deficiency resulted in altered Ago1/2 RNP assembly, shifting Ago1/2 association from P-bodies to actively translating polysomes. Finally, analysis of global translation in neurons led us to speculate that Ago—possibly via Stau2—needs to be properly balanced in order to ensure neuronal function and homeostasis. Importantly, our biochemical and cell biological study reveals a compensatory loop between two key RBPs providing new functional and mechanistic insight into neuronal Ago RNP assembly and RNAi.

MATERIALS AND METHODS

Plasmids

Plasmids expressing human Flag/HA-Ago1 (NM_012199.5, 214–2787 nt), Flag/HA-Ago2 (NM_012154.5, 128–2070 nt), Flag/HA-Ago2-S387A and Flag/HA-Ago2-824:34A were kindly provided by G. Meister (30) and subcloned into pEGFP-C3 (Clontech) or ptagRFP-C (Evrogen) under control of the CMV promotor. For luciferase assays 2× MS2 loops (31) or the 3′-UTR of rat *Rgs4* (position 728–2919 nt; NM_017214.1) were cloned 3′- of the Renilla open reading frame of the psiCHECK2 dual luciferase vector. The MS2 coat protein (MCP) (31) was cloned into ptagRFP-C (Evrogen) by replacing the tagRFP open reading frame and mouse Stau2 62kDa isoform (12) was inserted N-terminal to MCP. The plasmids expressing sh-resistant pCMV-tagRFP-Stau2 62kDa (12), pCMV-eGFP-Mov10 (NM001107711, 159–3173 nt) (20), psPAX2 (16) and pcDNA3.1-VSV-G (16) have been described previously. The pSUPERIOR.neo vector (Oligoengine) was used for expression of shRNAs; plasmids expressing shStau2 (32), shPum2 (33), shAgo2 (34), shHuR (34) have been described previously. For lentivirus expression, pCMV-eGFP-Ago2, pCamk2a-tagRFP-H1-shRNA, or pCamk2a-tagBFP-H1-shRNA were subcloned into lentiviral vector Fu3a. The shRNA oligo sequences were (5′–3′):

- shNTC_F: tccaaagttcgaatggtttttcaagagaaaccattcgaactttgga;
- shStau2_F: gatatgaaccaaccttcaattcaagagattgaaggttggttcatatc;

- shPum2_F: accaagttggtctggattcttcaagagagaatccagaccaacttggt;
- shHuR_F: gaagaggcaattaccagtttcattcaagagatgaaactggtaattgcctcttc;
- shAgo1_F: cgagaagaggtgctcaagaactgtgaagccacagatgggttcttgagcacctcttctcg;
- shAgo2_F: tgttcgtgaatttgggatcattgtacaatgatcccaaattcacgaaca.

Lentivirus production

Lentiviral particles for shNTC, shStau2, shPum2, shAgo2, shAgo1 and eGFP-Ago2 were generated from HEK-293T cells co-transfected with packaging plasmids psPAX2 and pcDNA3.1-VSV-G and the respective lentiviral Fu3a plasmid using calcium phosphate coprecipitation. After 48 h virus production, supernatants were filtered (0.45 μm PVDF Millex-HV; Millipore), concentrated by ultracentrifugation (65 000 × g, 140 min, SW 32 Ti rotor; Beckman Coulter) and resuspended in Opti-MEM™ (Life Technologies) (16).

Neuronal cell culture, transduction and transfection

All animals in this study were used according to the German Welfare legislation for Experimental Animals (LMU Munich, *Regierung von Oberbayern*). Rat hippocampal neuron cultures from embryos at day 17 (E17) of timed pregnant Sprague-Dawley rats (Charles River Laboratories) were generated as described previously (17). Briefly, E17 hippocampi were dissected, trypsinized and cells dissociated and plated on poly-L-lysine coated coverslips and cultured in NMEM + B27 medium (Invitrogen) with 5% CO_2 at 37°C. For cortical cultures, E17 cortices were trypsinized and dissociated, the cell suspension sequentially filtered through 100-, 70- and 40-μm cell strainers and then plated at a density of 100 000 cells/cm² on poly-L-lysine coated 60 or 100 mm dishes. For protein and RNA analysis, cortical neurons were transduced with lentiviral suspension at 9–10 days *in vitro* (DIV) and lysed at 13–14 DIV. For protein localization experiments, transient co-transfection of hippocampal neurons by calcium phosphate precipitation (35) was performed at 14 DIV, followed by fixation with 4 % PFA at 15 DIV.

Polysome profiling

Polysome profiling was performed as previously described (36) from neurons transduced at 10 DIV with eGFP-Ago2 and shNTC or shStau2, respectively. In brief, 5 million cortical cells per condition were incubated for 10 min with either cycloheximide (CHX, 355 μM) to stall ribosomes or with Harringtonine (3.7 μM) to induce ribosome run-off. Cells were homogenized in polysome lysis buffer (10 mM Tris–HCl pH 7.4, 150 mM NaCl, 5 mM $MgCl_2$, 1 vol% NP-40 (IGEPAL CA-630), 1% (w/v) sodium deoxycholate supplemented with 100 μg/mL CHX and 2 mM dithiothreitol) at 4°C, Lysates were precleared at 13 000 × g at 4°C for 5 min and subsequently loaded onto 18–50% (w/v) sucrose gradients (5 ml, 100 mM KCl, 5 mM $MgCl_2$, 20 mM HEPES pH 7.4). Gradients were spun at

35 000 rpm (SW55Ti rotor, Beckman Coulter) at 4°C for 1.5 h and fractionated (10 × 500 μl, Piston Fractionator, Biocomp) with continuous RNA absorbance detection at 254 nm. Protein extraction of 300 μl was performed using methanol/chloroform (37) and proteins were resolubilized in SDS loading buffer at 90°C for 3 min.

eGFP-Ago1/2 and eGFP-Mov10 protein localization

Analysis of eGFP-Ago1/2 or eGFP-Mov10 localization in dependence of Stau2, Pum2 or HuR depletion was performed in hippocampal neurons grown on coverslips. Neurons were transiently co-transfected at 14 DIV with the respective overexpression plasmids and shNTC, shStau2, shPum2 or shHuR expressing plasmids using calcium phosphate precipitation. Neurons were fixed with 4% PFA 16–20 h post transfection at 15 DIV. Coverslips were immunostained against Stau2 or Pum2, mounted on microscope slides with Fluoromount™ Aqueous Mounting Medium (Sigma), imaged and analyzed as described in the microscopy and image analysis section.

Puromycylation assay

Cortical neurons (2 million per condition) grown in 60 mm dishes, or hippocampal neurons grown on coverslips were transduced with lentiviruses expressing shNTC, shStau2, shAgo1, and/or shAgo2 at 8–9 DIV. The medium was refreshed after two days of lentivirus transduction. At 13–14 DIV, neurons were treated with 1 μM puromycin for 5 min, washed 2× with warm HBSS and lysed in 3xSDS loading buffer (cortical neurons for Western Blot) or fixed with 4% PFA for 10 min (hippocampal neurons for immunostaining). As control, cells were pretreated with 100 μg/ml cycloheximide for 10 min prior to addition of puromycin. Western Blot, immunostaining against puromycin, microscopy and image analysis were performed as described in the respective sections. Quantification of the puromycin intensity from Western Blot was performed by measuring the whole lane intensity normalized to αTubulin, for each biological replicate two technical replicates were performed. For hippocampal neurons, the average cell body intensity was measured of ≥35 healthy neurons per experiment and condition.

Western blotting

Samples were treated with 50 U Benzonase Nuclease (Merck) for 10 min and 3× SDS loading buffer was added, prior to heating to 65°C for 12 min. Proteins of equivalent number of neurons were resolved on 10% SDS-PAGE, transferred to nitrocellulose (pore size 0.2 μm) and subjected to immunoblotting with mouse anti-Ago2 (2E12-1C9) (1:500, WH0027161M1, Sigma), rabbit anti-Stau2 (1:500, selfmade (28)), rabbit anti-αTubulin (1:15 000, P1332Y, Abcam), rabbit anti-GFP (1:500, K3-184-2, kind gift from A. Noegel), mouse anti-Puromycin (1:500, 12D10, Millipore), or rabbit anti-Rpl7a (1:1000, Abcam) diluted in blocking solution (2% BSA, 0.1% Tween20, 0.1% sodium azide in TBS pH 7.5). After incubation with IRDye labelled secondary donkey anti-mouse, anti-rabbit, or anti-goat (IRDye 800CW or 680RD, Li-Cor),

all diluted 1:15 000 in blocking solution, membranes were imaged on an Odyssey CLx Imaging System (Li-Cor). Band intensities were quantified using Image Studio Lite software (Li-Cor) and normalized to αTubulin signal intensity.

RNA extraction, cDNA synthesis and qRT-PCR

Total RNA from cortical neurons was extracted using TRIzol (Invitrogen) or miRNeasy Mini Kit (Qiagen). cDNA was generated from 1 μg of DNase treated total RNA, using Superscript III reverse transcriptase (Invitrogen) with minor variation to the manufacturer's instructions. A mixture of 1.5 μM random primer mix (New England Biolabs) and 2.5 μM (dT)20 was used during cDNA synthesis. Quantitative real time PCR (qRT-PCR) was performed in duplicates from a 1:50 dilution of the stock cDNA using a home-made SYBR Green Master Mix (12), with the LightCycler 96 System (Roche). Only primers with an optimized efficiency of 95–105% were used. The $2^{-\Delta\Delta Ct}$ method implemented in the LightCycler Software (Roche) was used to calculate differences in RNA levels relative to peptidylprolyl isomerase A (*Ppia*) mRNA. The sequences of the qRT-PCR primers were (5′–3′):

- Ppia_F: gtcaaccccaccgtgttctt; Ppia_R: ctgctgtctttggaactttg;
- Drosha_F: ctacacggtggccgtttact; Drosha_R: caatgaaccgcttctgatga;
- Dicer_F: gcaaggaatggactctgagc; Dicer_R: gtacacctgccagaccacct;
- Stau2_F: agttgcgactggaacaggac; Stau2_R: tggaccactccatcctttgt;
- Ago1_F: caacatcactcacccgtttg; Ago1_R: gcaggtgctgggatagagac;
- Ago2_F: acaagctggttttgcgctac; Ago2_R: ttgctgatctcctcttgccg;
- Pum2_F: atgggagcagctctttgact; Pum2_R: gatgagccaaatccactgagag.

Immunostaining

For immunostaining neurons were washed twice with warm HBSS and then fixed with warm 4% PFA in HBSS for 10 min. Fixed cells were washed thrice with HBSS and permeabilized with 0.1% Triton X-100 in DPBS for 5 min and blocked for at least 30 min in blocking solution (2% FCS, 2% BSA, 0.2% fish gelatin (Sigma) in DPBS). The following primary antibodies were used overnight in 10 vol% blocking solution in DPBS: mouse anti-Ago2 (2E12-1C9) (1:500, WH0027161M1, Sigma), rabbit anti-Stau2 (1:500, selfmade (28)), mouse anti-Stau2 (1:500, selfmade (28)), mouse anti-Puromycin (1:500, 12D10, Millipore), mouse anti-Dcp1a (1:500, Sigma), rabbit anti-Ddx6 (1:500 (Rck), MLB), mouse anti-Pum2 (1:10 000, Abcam). The following secondary antibodies were used for 2 h in 10 vol% blocking solution in DPBS: donkey anti-mouse or rabbit AF488-, AF555- or AF647-conjugated antibodies (all Invitrogen). Coverslips were mounted on microscope slides with Fluoromount™ Aqueous Mounting Medium (Sigma).

Sholl analysis

Hippocampal neurons grown on coverslips were transiently transfected at 11 DIV with plasmids expressing fluorescent reporters and shNTC, shStau2, shAgo1 and/or shAgo2. Three days after transfection, neurons were washed with warm HBSS and fixed with 4 % PFA for 10 min. Images were acquired as described below and the eGFP fluorescent reporter signal was used as marker to visualize the dendritic tree of transfected neurons. Using ImageJ, images were converted into 8 bit and a threshold was set for clear differentiation between dendrites and background. Unspecific background pixels were removed, a line between the center of the cell body and the furthest dendritic signal was drawn as basis for the Sholl analysis plugin in ImageJ (10 μm ring step size) that automatically counted intersections between dendritic branches and individual concentric rings.

Microscopy and image analysis

Images were acquired using Zeiss Zen software on a Zeiss Z1 Axio Observer microscope including a 63× Plan-Apochromat oil immersion objective (1.40 NA), a COL-IBRI.2 LED and an HXP 120 C light source and the Axiocam 506 mono camera. Neurons were selected for cell morphology and viability as well as for expression of plasmids or lentiviruses and images were taken in the dendritic plane. For eGFP-Ago1/2 and eGFP-Mov10 protein localization experiments, z-stacks of whole neurons were acquired (30 planes with 0.26 μm step-size) and a z-projection of the maximum intensity was performed in ImageJ. The number of eGFP-Ago1/2, eGFP-Mov10, Dcp1a and Ddx6 particles per neuron were manually counted using the multipoint tool in ImageJ. For cell body fluorescence intensity quantification of eGFP-Ago2, or puromycin, Stau2 and Pum2 protein signal, the measure function in the Zeiss Zen software was used and a region of interest was drawn by hand based on the phase contrast image. Analysis of colocalization between endogenous Ago2, Stau2, Dcp1a and Ddx6 was performed by acquisition of z-stacks of whole neurons (35 planes with 0.22 μm step-size), followed by deconvolution using the Zeiss Zen software deconvolution module, with default settings of the constrained iterative method. Colocalization analysis was performed blind using ImageJ within the first 15 μm of the dendrite (proximal) and within a 15 μm box ≥20 μm away from the cell body (distal). For all experiments, ≥15 neurons per condition from at least three independent biological experiments were quantified.

Dataset comparison and gene ontology analysis

Gene ontology overrepresentation analysis was done using the statistical overrepresentation test of the PANTHER classification system (http://www.pantherdb.org) (38). Protein network analysis was done using STRING database (https://string-db.org) (39). Comparison of Stau2 related MS datasets with P-body enriched genes were performed using R studio based on the Gene names.

Statistical analysis

Microsoft Excel, Prism5 and R software (ggplot2) were used for data processing, plotting and statistical analy-sis. Figures represent mean ± standard error of the mean (SEM) of at least three independent biological replicates. Asterisks and hashtags represent *p*-values obtained by one-way ANOVA and either paired or unpaired two-sided Student's t-test using the mean values per experiment (*$P < 0.05$, **$P < 0.01$, ***$P < 0.001$, ****$P < 0.0001$), if not stated otherwise.

RESULTS

Ago1/2 and RISC effector proteins are upregulated in Stau2 depleted neurons

Recently, we have performed label-free quantitative mass spectrometry to characterize proteome changes in primary cortical neurons upon depletion of Stau2 (36). This allowed us to analyze possible changes of RBP levels in detail, which would give us first insights into the underlying dynamics of RNP remodeling (20,36). Using gene ontology (GO) analysis, we found a statistically significant enrichment of miRNA associated biological processes in the proteome of Stau2-deficient neurons (Figure 1A). In particular, we observed a concerted upregulation of the RISC effector proteins Ddx6, Dcp1a and Edc4 and especially Ago1 and Ago2 proteins upon Stau2 depletion (Figure 1B, Supplementary Figure S1A). The depicted protein interactor scheme (Figure 1B inset) suggests that these significantly upregulated RBPs are functionally connected with each other (23,40). This upregulation appears to be predominantly regulated at the protein level, as there was no corresponding significant increase of *Ago1* and *Ago2* mRNA levels in cortical neurons deficient for Stau2 (Figure 1C). This prompted us to inquire whether Stau2 possibly altered expression or translation of upregulated miRNA associated genes via direct RNA-binding. We compared the list of upregulated proteins with published Stau2 target RNA datasets from RNA immunoprecipitation (16) and individual-nucleotide resolution UV crosslinking and immunoprecipitation (iCLIP) (12) experiments (both from embryonic neuronal tissue). Notably, the mRNAs coding for Ago1, Ago2, Ddx6, Dcp1a and Edc4 were not enriched in those datasets, suggesting that Stau2 does not regulate their expression through direct RNA-binding (Figure 1D, Supplementary Figure S1B). Several lines of evidence, however, suggest a possible link between Stau2 and the miRNA machinery: (i) Staufen has been linked to processing of small interfering RNAs in coleopteran insects (41); (ii) nuclear export of the Stau2 62 kDa isoform is dependent on the miRNA-export factor Exportin5 (42); and (iii) mRNAs of miRNA processing factors *Drosha* and *Dicer* were upregulated in Stau2 deficient neurons (16) (Supplementary Figure S1C).

To test whether Stau2 indeed regulates mature miRNA levels, we performed small RNA sequencing from Stau2 deficient cortical neurons (Supplementary Figure S1D–G). Of the total detected miRNA population, 43 miRNAs (8 %) were differentially regulated with the majority being down-regulated (Supplementary Figure S1E, F). However, while the expression of some miRNAs is significantly changed, we did not observe an overall reduction in total miRNA abundance upon Stau2 KD (Supplementary Figure S1G). This is in accordance with previous results from *C. elegans* deficient for Staufen (43). Based on these results, we conclude
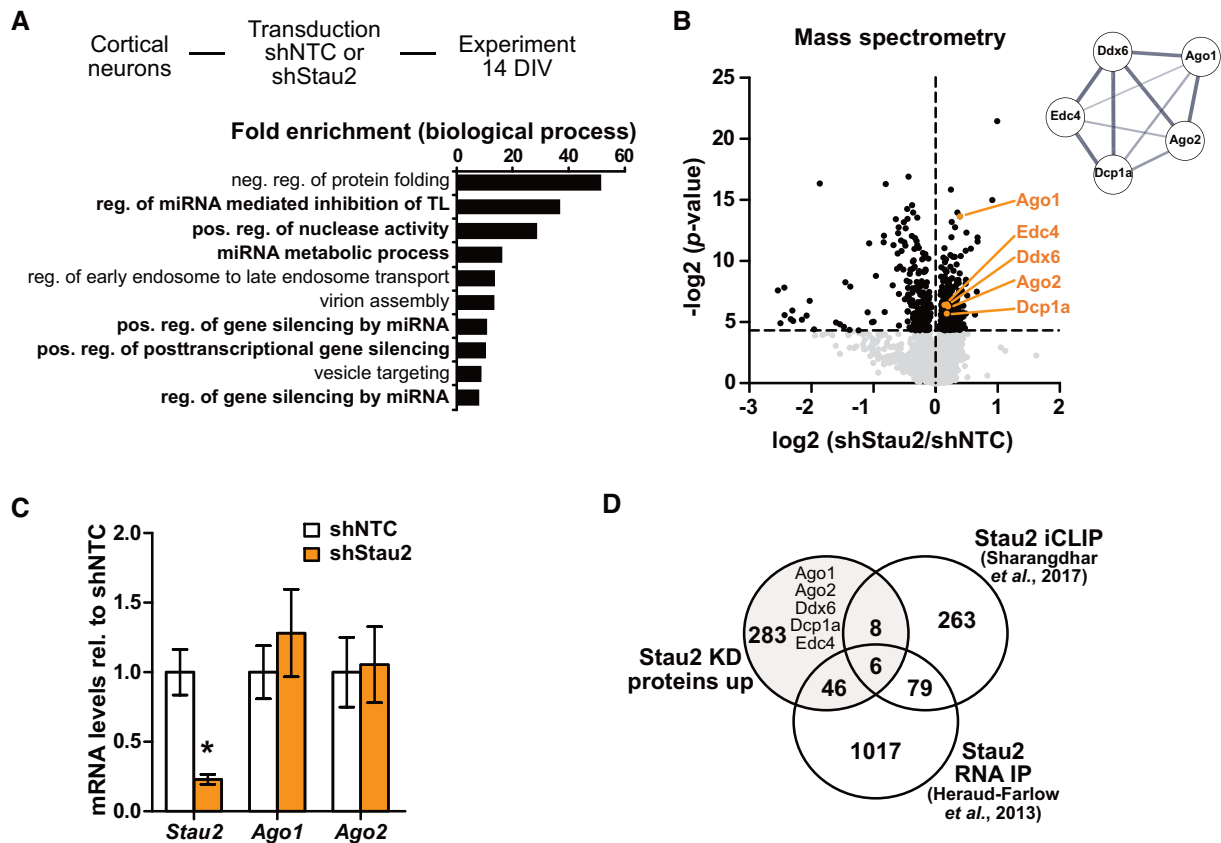
Figure 1. Stau2 depletion leads to upregulation of Ago1/2 and RISC effector proteins. (**A**) Gene ontology (GO) overrepresentation analysis (PANTHER, biological process) of all significantly upregulated proteins from primary rat cortical neurons deficient for Stau2 from Schieweck *et al.* (36). (**B**) Volcano plot displaying protein levels measured by quantitative mass spectrometry and protein network analysis (STRING database) of highlighted significantly upregulated genes (orange; *p*-value as criteria) from Schieweck *et al.* (36); unpaired two-tailed Student's *t*-test. (**C**) Quantification of *Stau2*, *Ago1* and *Ago2* mRNA levels using qRT-PCR from cortical neurons at 14 DIV transduced with shNTC or shStau2 at 10 DIV, normalized to *Ppia* and shNTC; paired two-tailed Student's *t*-test. (**D**) Venn diagram comparing proteins significantly upregulated upon Stau2 KD (36), RNAs enriched in Stau2 RNA-IPs (16), or Stau2 targets identified by iCLIP (12). Error bars are $\pm$ SEM from ≥ 3 independent biological experiments; asterisks represent *P*-values (*$P < 0.05$). DIV, days *in vitro*; NTC, non-targeting control; TL, translation; KD, knock down; iCLIP, individual-nucleotide resolution cross-linking and immunoprecipitation.

that the upregulation of Ago1/2 and its effector proteins upon downregulation of Staufen is not caused by changes in global miRNA abundance, but might be the result of a more sophisticated regulation of a specific subset of miR-NAs and/or of other miRNA independent mechanisms, such as posttranslational modifications or protein stability.

Stau2 co-localizes with Ago2 in distal dendrites

In HEK-293 cells, Stau2 as well as the upregulated miRNA associated proteins are found to be enriched in LSM14-positive P-bodies (11) (Figure 2A). We therefore investigated whether Stau2, Ago2 and Ddx6 co-localize in the same RNA granules in neurons with a particular focus on proximal and distal dendritic segments (Figure 2B). In the proximal segment, Ago2 showed strong colocalization with Ddx6 (90 ± 5%) while colocalization with Stau2 was more subtle (23 ± 5%) (Figure 2C). These results are in line with previous colocalization analysis and live cell imaging data showing transient interactions between Stau2 and Ago2 (28). Interestingly, this pattern changed in distal dendrites and colocalization of Ago2 with Stau2 increased signifi-

cantly to 45 ± 6%. Together, this suggests that both Stau2 and Ago2 proteins indeed interact with each other. Interestingly, this interaction seems to be localization-dependent and might take place rather in dendritic RNPs than in somatic P-bodies.

Stau2 selectively regulates Ago1/2 localization to P-bodies

Next, we investigated whether Stau2 might affect Ago2 protein localization in primary hippocampal neurons. Since the interaction of Stau2 and Ago2 seemed to be dependent on the localization, we hypothesized that Stau2 deficiency could selectively affect Ago2 RNP assembly. Similar to endogenous Ago2 (Figure 2B), eGFP-Ago2 predominantly yielded a granular pattern and colocalized with endogenous Dcp1a and Ddx6 in control conditions (shNTC) in mature neurons (Figure 3A,B). Upon depletion of Stau2 by RNA interference using an shRNA against Stau2 (Supplementary Figure S2A) (16), eGFP-Ago2 disassembled from P-bodies and yielded a diffuse expression pattern (Figure 3A). This decrease in puncta number per cell is statistically significant: 46 ± 7 to 10 ± 4 eGFP-Ago2 particles
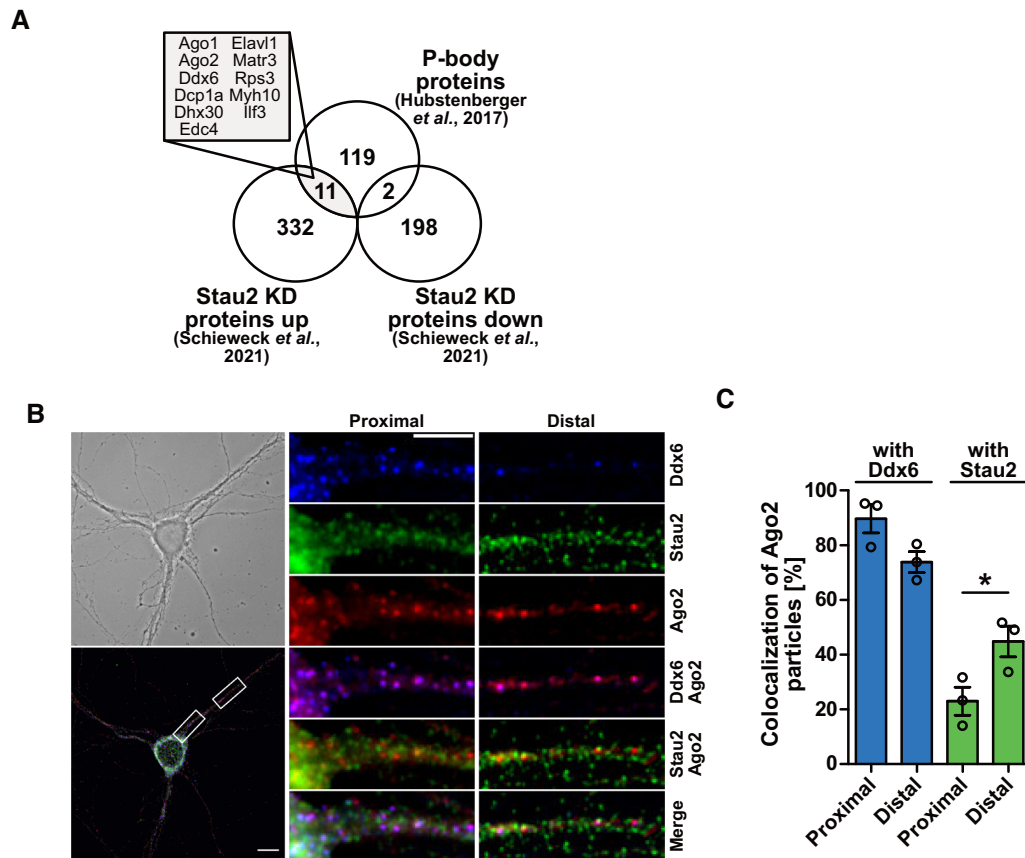
Figure 2. Ago2 and Stau2 significantly co-localize. (**A**) Venn diagram comparing significantly altered proteins upon Stau2 KD (36) and proteins enriched in P-bodies (11). (**B**) Representative phase contrast and pseudocolored, deconvolved fluorescent images of hippocampal neurons (15 DIV) stained for Ago2, Ddx6 and Stau2, respectively. Scale bar is 10 μm and 5 μm for insets. (**C**) Quantification of co-localization between endogenous Ago2 particles and Ddx6 or Stau2 particles in proximal (first 15 μm) or distal (≥20 μm from cell body) dendrites. Error bars are ± SEM from ≥3 independent biological experiments and ≥20 cells per replicate; asterisks represent *P*-values (*$P < 0.05$). Paired two-tailed Student's *t*-test. KD, knock down; P-body, processing body.

per cell with a *P*-value of 0.0294 (Figure 3C). The frequency distribution of the number of eGFP-Ago2 particles per cells nicely reflects this effect (Supplementary Figure S2B). Quantification of the eGFP-Ago2 intensity in the cell body (Figure 3A) revealed a similar increase upon Stau2 depletion (Supplementary Figure S2C) as detected for endogenous Ago2 in both the mass spectrometry and Western Blot analyses (Figure 1B, Supplementary Figure S1A). Together, our data thereby further substantiate posttranscriptional upregulation of Ago2. Interestingly, Ago1, another Ago protein family member, that was even stronger upregulated as Ago2 in Stau2 depleted neurons (Figure 1B), showed a similar change in the localization and distribution pattern upon downregulation of Stau2 as compared to eGFP-Ago2 (Figure 3D,E; Supplementary Figure S2D). This indicates that the regulation is not Ago2 specific, but is apparently true for other Ago proteins. Furthermore, we examined the Stau2 dependent localization of Dcp1a (P-body marker) and Mov10 (known Ago2 and Stau2 interacting protein). Importantly, localization of both proteins remained unaffected by Stau2 depletion (Figure 3F, Supplementary Figure S2F,G), suggesting that the overall formation of P-bodies is unaffected.

Phosphorylation of Ago2 has been shown to regulate its P-body localization and affinity to RISC associated proteins (Ago2 S387) (44,45) as well as its affinity to target mRNAs (Ago2 S/T824:34) (30,46). We therefore asked whether these two well characterized Ago2 phosphomutants might affect the Stau2-dependent Ago2 localization in primary neurons (Supplementary Figure S2H–K). As in the wildtype eGFP-Ago1/2 localization assay, we co-expressed eGFP-Ago2 alanine phosphomutants (S/T824A and S387A) and sh constructs in hippocampal neurons and quantified the number of eGFP particles per cell. In control conditions (shNTC), both phosphomutants localized to P-bodies and displayed a similar particle number per cell as wildtype eGFP-Ago2 (Figure 3C). Loss of Stau2 resulted in a strong and significant reduction of eGFP-Ago2 S/T824:34A as well as eGFP-Ago2 S387A particles, mimicking the pattern observed in wildtype eGFP-Ago2 (Figure 3C). Importantly, none of the phosphomutants resulted in significant changes compared to wildtype Ago2 arguing that the observed Stau2-dependent regulation is likely to be independent of posttranslational modifications of Ago2.

We next investigated whether the observed disassembly of Ago2 from P-bodies can be rescued by reintroducing Stau2
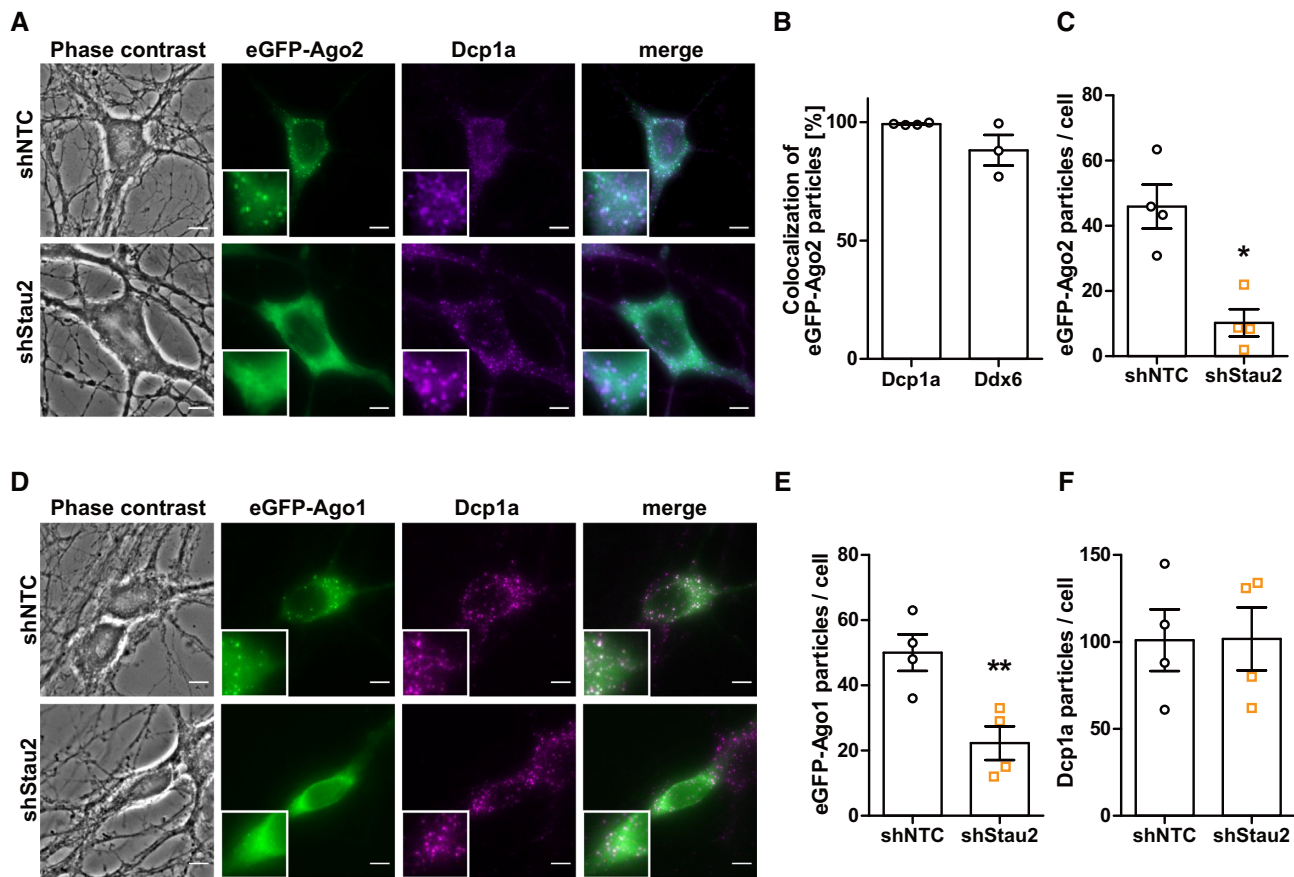
Figure 3. Stau2 regulates Ago1/2 localization to P-bodies. (A, D) Representative phase contrast and pseudocolored fluorescent images of hippocampal neurons co-transfected at 14 + 1 DIV with eGFP-Ago2 (**A**) or eGFP-Ago1 (**D**), shNTC or shStau2 constructs and immunostained against Dcp1a. (**B**) Quantification of co-localization between eGFP-Ago2 particles and Dcp1a or Ddx6. (**C**) Quantification of eGFP-Ago2 particles per cell. (D) Representative images as in (A) of hippocampal neurons transfected with eGFP-Ago1. (**E**) Quantification of eGFP-Ago1 particles per cell. (**F**) Quantification of Dcp1a particles per cell. Error bars are ± SEM from ≥3 independent biological experiments (shown as individual symbols) with ≥15 cells per replicate and condition; asterisks represent *P*-values (*$P < 0.05$, **$P < 0.01$). Paired two-tailed Student's *t*-test. Scale bar is 5 μm. DIV, days *in vitro*; NTC, non-targeting control.

protein. First, overexpression of an sh-resistant tagRFP-Stau2^R (17) in control conditions (shNTC) significantly increased the average number of eGFP-Ago2 particles per cell (60 particles), compared to cells expressing only tagRFP (38 particles). Furthermore, overexpression of tagRFP-Stau2^R in the presence of shStau2 partially rescued eGFP-Ago2 localization to P-bodies (Figure 4A, B). In order to ensure that the observed re-localization is not caused by mere overexpression of an exogenous Ago-dependent shRNA (shStau2), we repeated the experiment by co-expressing shRNAs against the RBPs Pum2 and HuR, respectively (Figure 4C, D; Supplementary Figure S3). Rewardingly, overexpressing exogenous shRNAs did not affect eGFP-Ago1/2 localization in neurons. Together, these data suggest that Stau2 selectively regulates the assembly of Ago RNPs, but not of other P-body enriched proteins.

Ago2 associates with translating polysomes upon Stau2 depletion

Ago proteins have been linked to translation inhibition as well as RNA degradation (22). While P-bodies are thought to be sites of RNA storage, RNAi mediated translation con-

trol appears to be generally independent of these granules (47,48). In this context, it is interesting to note that Ago2 can associate with polysomes at the endoplasmic reticulum and in the cytosol (49), where it inhibits (50) or promotes translation (51), respectively. As we observed disassembly of Ago2 from P-bodies upon Stau2 depletion, we were interested whether cytoplasmic Ago2 were to associate with polysomes. Therefore, we performed polysome profiling (52), a method where translating ribosomes are frozen on the mRNA by incubating neurons with the translation inhibitor cycloheximide, followed by lysis and fractionation on a sucrose gradient (Figure 5A). Western Blot analysis of the profiling fractions revealed that both eGFP-Ago2 and Stau2 comigrate with polysomes (Figure 5B). Interestingly, eGFP-Ago2 comigration significantly increased in Stau2 deficient neurons (Figure 5B, C), while the ribosomal marker Rpl7a remained unchanged. Ribosome run-off of actively translating polysomes by pretreatment of neurons with the translation initiation inhibitor harringtonine resulted in a shift of Rpl7a as well as eGFP-Ago2 towards monosomes (Figure 5D,E), compared to cycloheximide-treated neurons (Figure 5B, C). This indicates that eGFP-Ago2 migration indeed depends on actively translating
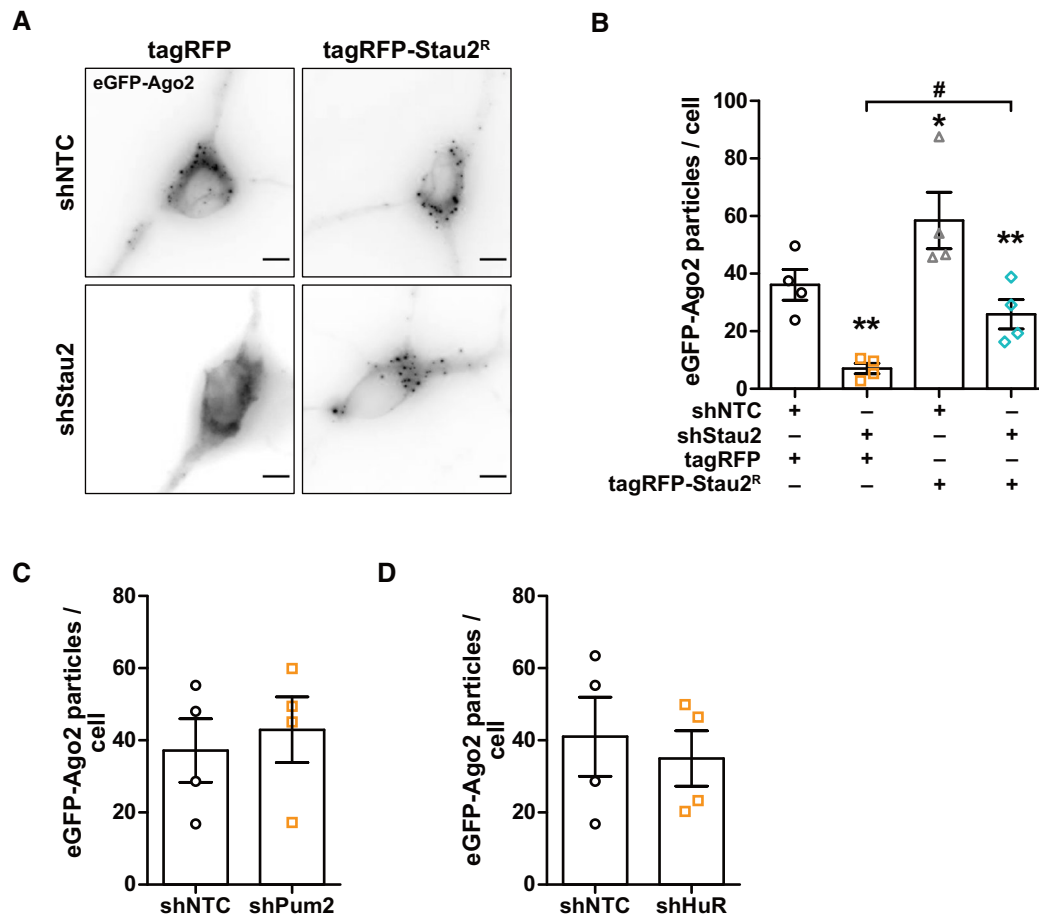
Figure 4. Ago2 localization is Stau2 specific. (**A, B**) Representative inverted fluorescent images and quantification of hippocampal neurons co-transfected at 14 + 1 DIV with eGFP-Ago2, shNTC or shStau2, and tagRFP or sh-resistant tagRFP-Stau2^R constructs. (B) Quantification of eGFP-Ago2 particles per cell. (**C**) Quantification of eGFP-Ago2 particles per cell from hippocampal neurons co-transfected at 14 + 1 DIV with eGFP-Ago2 and either shPum2 or shNTC. (**D**) Quantification of the number of eGFP-Ago2 particles per cell from hippocampal neurons co-transfected with either shHuR or shNTC at 14 + 1 DIV. Error bars are ± SEM from four independent biological experiments (shown as individual symbols) with ≥15 cells per replicate and condition; asterisks (to shNTC/tagRFP) and hashtags (between shStau2/tagRFP and shStau2/tagRFP-Stau2^R) represent *P*-values (*$P < 0.05$, **$P < 0.01$). Paired two-tailed Student's *t*-test. Scale bar is 5 μm. NTC non-targeting control; Stau2^R, sh-resistant form of Stau2.

polysomes. In other cell types, treatment with cycloheximide leads to disassembly of P-body markers (53,54). If this were also the case with our cycloheximide treatment in primary neurons, the polysome profiling data would be compromised since Ago localization would change due to P-body disassembly. Interestingly, the granule assembly of both Dcp1a as well as Ddx6 were not affected by cycloheximide treatment of primary neurons, using identical conditions as used for polysome profiling, 10 min and 355 μM (Figure 5F, G). Additionally, recent in-depth data on Ddx6 granule assembly show its dependence on both the neuronal activity as well as the translational state (Bauer *et al.*, 2022, *Nature Comm.*, *in press*). Furthermore, as a pilot experiment, we explored the molecular basis of the interaction between Stau2 and Ago on the target level by performing Ago2-IP experiments in the presence and absence of Stau2 (Supplementary Figure S4). Here, we found increased Stau2 target association for *Rgs4* (16), *Rhoa* (19) and *Calm3* (12) with Ago2 upon Stau2 depletion (Supplementary Figure S4D). It is tempting to speculate that these targets become available for Ago2 binding upon release from Stau2 RNPs.

Together, our data suggest that Stau2 depletion results in an increased association of Ago2 with some Stau2 target mRNAs as well as with actively translating polysomes. The latter observation matches the disassembly of Ago2 from P-bodies upon Stau2 depletion, since P-bodies are reported to be free of polysomes (11).

Ago1/2 and Stau2 act antagonistically on global translation

Ago proteins and RISC inhibit translation (21). In some cases, however, they have been reported to promote translation (51,55). We therefore set out to test whether increased association of Ago with polysomes upon Stau2 depletion resulted in inhibition or rather in stimulation of global translation. Therefore, we designed lentiviruses harboring shRNAs against Ago1 and Ago2 and tested the effect of Ago1/2 depletion, as well as Stau2 depletion (Supplementary Figure S5A), on global translation in cortical and hippocampal neurons using the puromycylation assay (56). Puromycin binds to actively translating ribosomes, resulting in termination of translation and release of puromycin
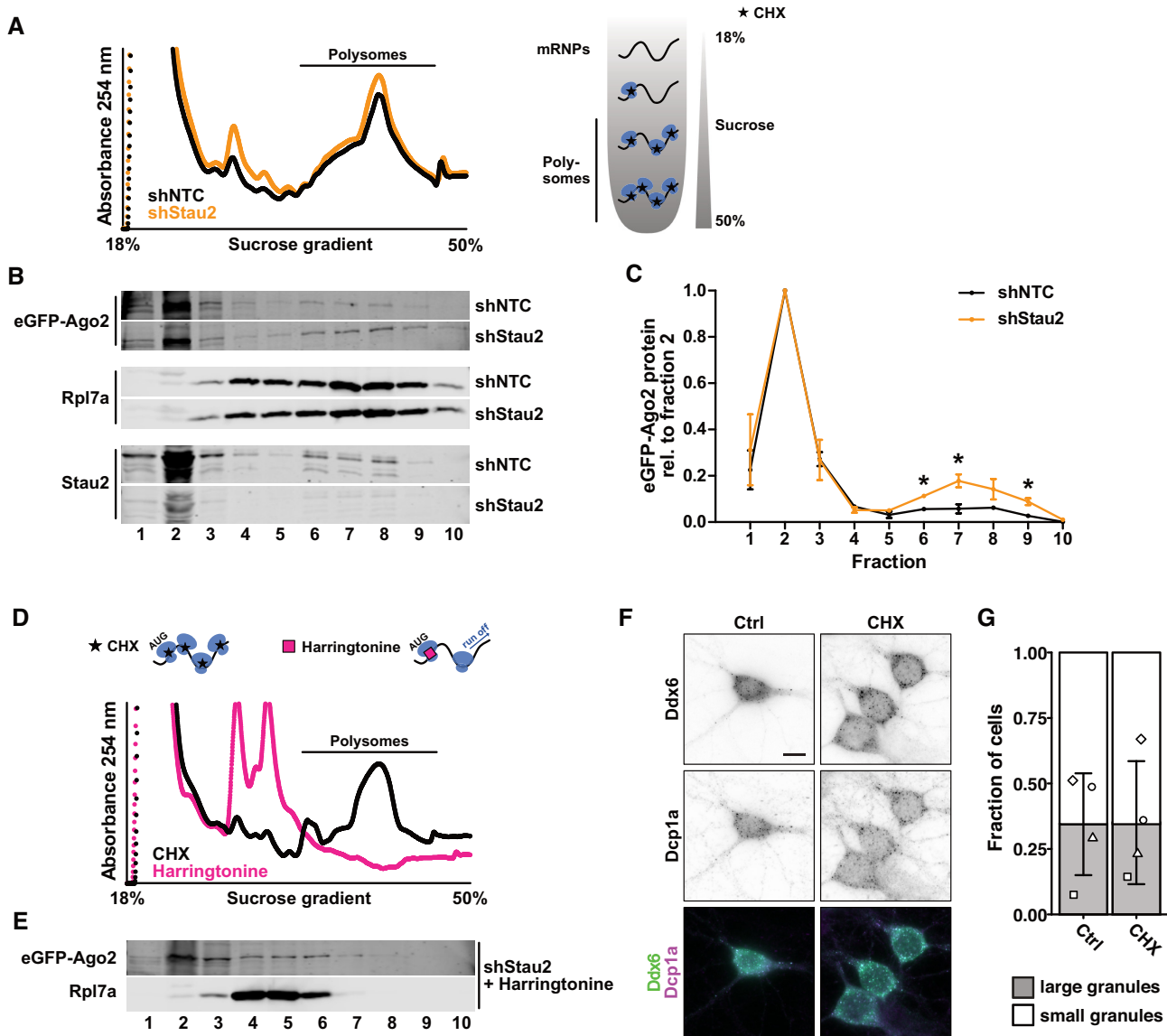
Figure 5. Ago2 associates with translating polysomes in Stau2 depleted neurons. (**A**) Polysome profiles of post-nuclear lysates from cortical neurons treated with translation inhibitor cycloheximide (CHX) at 14 DIV and transduced at 10 DIV with lentiviruses expressing eGFP-Ago2 and shNTC or shStau2 and experiment outline. (**B**) Representative Western Blots of polysome profiles, immunoblotted for eGFP, Stau2 and Rpl7a (serving as ribosome marker). (**C**) Quantification of Western Blot eGFP-Ago2 protein intensities from three independent polysome profiling experiments, normalized to fraction 2. (**D**) Polysome profiles from cortical neurons transduced as in A pretreated with Harringtonine and experimental outline. Harringtonine inhibits the first round of translation elongation after initiation. (**E**) Representative Western Blots of polysome profiles from cortical neurons treated with Harringtonine and transduced with shStau2 and eGFP-Ago2, immunoblots for eGFP and Rpl7a are shown (western blots correspond to same biological replicate as shown in B). (**F**) Representative deconvolved fluorescent images (pseudocolored) of hippocampal neurons (22 DIV) treated with DMSO (Ctrl) or 355 µM CHX for 10 min and stained for Dcp1a and Ddx6. Scale bar is 10 µm. (**G**) Quantification of neurons from (F), categorized into cells with small or large granules. Error bars are ± SEM from ≥3 independent biological experiments; asterisks represent *P*-values (*$P < 0.05$). Paired two-tailed Student's *t*-test. DIV, days *in vitro*; NTC, non-targeting control; CHX, cycloheximide; DMSO, dimethylsulfoxide.

labelled peptides that can be detected by puromycin antibodies. Pretreatment of neurons with the translation inhibitor cycloheximide prevented puromycin incorporation (Figure 6A, B), indicating that the assay indeed detected active translation. Downregulation of Ago1/2 protein levels resulted in upregulated global translation in hippocampal neurons detected by immunostaining against puromycin (Figure 6C, D). On the contrary, depletion of Stau2 resulted in an overall decrease of global translation. Finally, co-expression of shAgo1/2 and shStau2 resulted in a res-

cue of translation levels comparable to control (shNTC). These effects could also be reproduced in cortical neurons by Western Blot analysis (Supplementary Figure S5B).

As depletion of Stau2 caused an overall decrease in translation, we wanted to explore whether Stau2 alone would promote gene expression in cells. For this, we performed MS2 tethering assays and included a validated Stau2 target mRNA from neurons, *Rgs4* (16,57), as positive control. Similar to previous results from neurons (16), overexpressing tagRFP-Stau2 in HeLa cells caused a significant
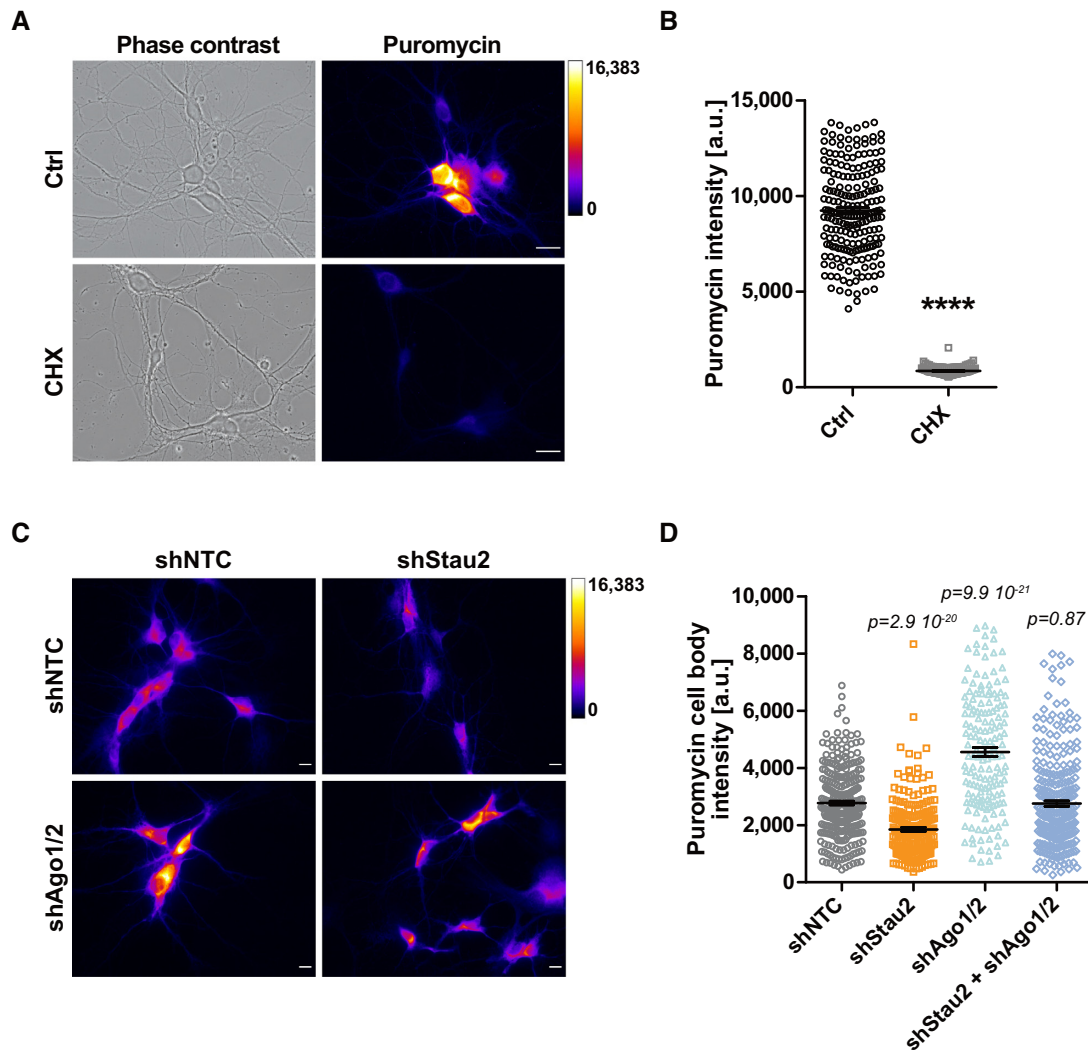
Figure 6. Stau2 and Ago1/2 oppositely regulate translation. (**A**) Representative fluorescent images of hippocampal neurons and dot plot (**B**) of the cell body puromycin signal intensity from two biological replicates treated with translation inhibitor CHX or with DMSO as control (≥35 cells per replicate and condition; cells shown as individual symbols). Scale bar is 20 μm. (**C**) Representative fluorescent images of hippocampal neurons transduced with lentiviruses expressing shNTC, shStau2, or shAgo1/2 at 8–9 DIV and treated with puromycin prior to fixation at 13–14 DIV. Scale bar is 10 μm. (**D**) Dot plot of the cell body puromycin signal intensity from four biological replicates (≥ 40 cells per replicate and condition; cells shown as individual symbols). Puromycin fluorescent intensity is shown as pseudocolored grey values. Error bars are ± SEM; asterisks represent *P*-values (****$P < 0.0001$). Unpaired two-tailed Student's *t*-test. DIV, days *in vitro*; Ctrl, control; CHX, cycloheximide; NTC, non-targeting control.

increase in *Rgs4* 3′-UTR luciferase reporter activity (Supplementary Figure S5C). When we tethered tagRFP-Stau2 fused to the MS2-coat binding protein to the luciferase reporter mRNA by simply adding 2 MS2 binding sites without any Rgs4 sequence elements, we observed a significant increase. Importantly, however, mere overexpression of untethered tagRFP-Stau2 did not result in changes of MS2 reporter expression arguing against unspecific binding of Stau2 to the MS2 stem loops. These data suggest that Stau2 is likely to also act independently of its effect on Ago1/2 to promote translation.

Stau2 and Ago1/2 balance neuronal branching

In conclusion, the results presented in this study are all consistent with the idea of opposing functions of Stau2 and Ago1/2 in neuronal posttranscriptional gene expression. This hypothesis and the biological relevance of this interaction is further strengthened by experiments in developing neurons, in which we investigated the potential of RBPs affecting dendritic arborization. Loss of Stau2 profoundly increased neuronal branching, while knockdown of Ago1/2 led to reduction of branching complexity (Figure 7A–C). Interestingly, individually downregulating either Ago1 or Ago2 did not result in altered dendritic branching (Supplementary Figure S6A,B). In line with the above-mentioned experiments, double knockdown of both Stau2 and Ago1/2 was sufficient to restore control dendritic complexity. We therefore like to propose that expression and RNP assembly of Ago proteins—likely via Stau2—need to be properly balanced to ensure neuronal homeostasis.
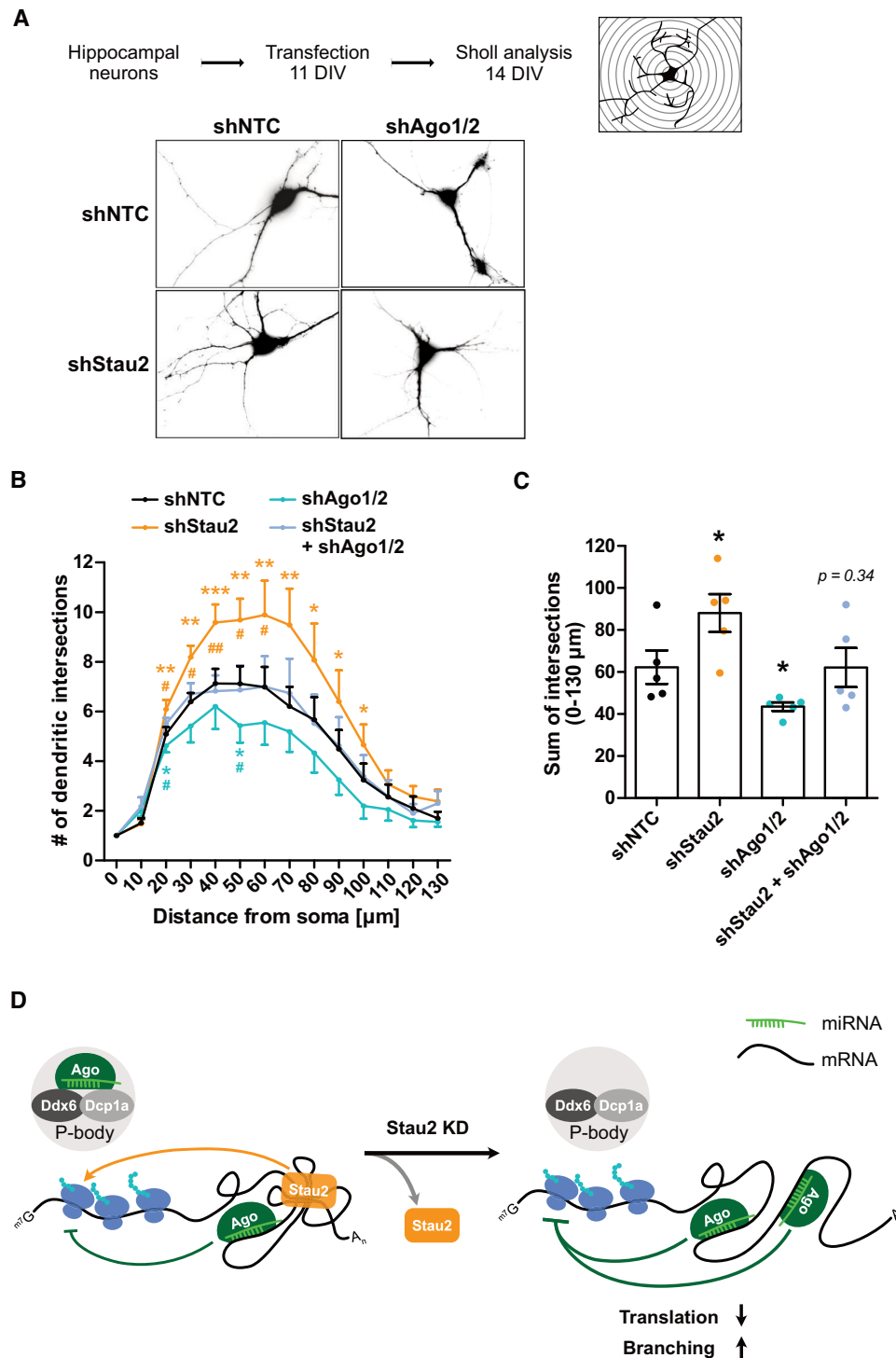
Figure 7. Balanced Stau2/Ago1/2 levels are important for neuronal branching. (**A**) Experiment outline and representative inverted eGFP fluorescent images of hippocampal neurons transfected at 11 DIV with respective shRNA constructs and fixed at 14 DIV for Sholl analysis. (**B**) Quantification of intersections between neuronal branches and concentric rings. (**C**) Dot plot showing the sum of intersections over all concentric rings. (**D**) Proposed working model of Stau2 governed Ago1/2 RNP assembly. In addition to Ago localization to P-bodies, Stau2 and Ago can also be present in smaller RNA particles distinct from classical P-bodies. Stau2, by preferentially binding complex RNA secondary structures, reduces the accessibility of miRNA binding sites. In the absence of Stau2, Ago proteins are now able to hijack these mRNAs with altered secondary structures. This may result in the observed mis-localization of Ago from P-bodies to the neuronal cytosol. Consequently, the remodeling of mRNPs in Stau2 depleted neurons is likely to yield in decreased overall translation in neurons (depicted by green inhibitory lines) and correlates with increased dendritic branching. It is important to note, that Stau2 may also has an Ago-independent effect on translation (depicted by orange arrow). Error bars are $\pm$ SEM from five independent biological experiments (shown as individual dots) with $\geq$ 20 cells per replicate and condition; asterisks (to shNTC) and hashtags (to shStau2 + shAgo1/2) represent p-values (*$P < 0.05$, **$P < 0.01$, ***$P < 0.001$). Paired two-tailed Student's t-test. DIV, days *in vitro*; NTC, non-targeting control; KD, knockdown; miRNA, mRNA, messenger RNA; microRNA.

DISCUSSION

It is now widely accepted in the field that RBPs do not act as separate players, but rather as interdependent factors jointly determining the fate of an RNA (2,29). Depending on the combination of both RNA sequence and structure elements that regulate RBP assembly, the action of individual RBPs can differ for different target RNA. For example, the AU-rich binding protein family Elavl has been shown to act synergistically as well as antagonistically with miRNAs/Ago on target RNAs (29,34,58). Here, we have taken an alternative approach by investigating the consequences of depleting a single RBP, Stau2, on the neuronal RBPome (36). Ago and RISC associated proteins were found to be collectively upregulated under those conditions. Together with our findings on the Stau2-specific Ago disassembly from P-bodies and increased association with polysomes, our data suggest Stau2 dependent regulation of Ago containing RNP assembly and composition. We therefore hypothesized whether this Stau2 dependent regulation could be caused by different molecular mechanisms, from (i) altered global miRNA abundance to (ii) changes in the phosphorylation state of Ago up to (iii) altered accessibility of miRNA binding sites in Stau2 target RNAs. The expression of proteins involved in miRNA processing and RISC assembly is tightly coupled to global miRNA abundance. As Stau2 binds to dsRNA and especially complex, extended RNA structures (12,32,59), potential binding to precursor miRNAs could therefore alter global miRNA processing. Furthermore, Stau2 has been previously connected to the small RNA processing pathway (41,42). We could exclude the first two proposed mechanisms by performing small RNA sequencing and by testing existing, well characterized phosphomutants of the two major Ago2 phosphorylation sites S387 and S/T824:34 (Supplementary Figures S1G, S2H–K). This led us to our third hypothesis where Ago—upon depletion of Stau2—hijacks previously inaccessible miRNA binding sites in the Stau2 target RNA pool (see our proposed model in Figure 7D). Under wildtype conditions, an equilibrium between P-body associated and diffuse cytosolic Ago exists. Upon depletion of Stau2, however, Ago dissociates from P-bodies and targets previously inaccessible miRNA binding sites in the Stau2 target RNA pool. Stau2 therefore critically regulates the RNP assembly of Ago. A similar mechanism based on structure-dependent RNA accessibility, however with an opposite outcome, has been reported for the RBP Pum1 and p27-3′-UTR (60) as well as recently for ribosomes (61). Pum1 binding or translation temporarily unfolds RNA structures in the 3′-UTR or coding sequence thereby enabling small RNA binding to the mRNA. In our model, Stau2—through binding to complex RNA structures—prevents RISC assembly on a specific subset of RNAs, which in turn modulates RNA fate. Eventually, this results in increased translation and/or RNA stability, which is in line with our findings that overall translation is decreased in Stau2 depleted neurons (Figure 7D), and that this effect can be rescued by knockdown of Ago1/2. It is likely that Stau2 has an additional Ago-independent effect on translation, as shown in *Drosophila* (62).

We also observed this complementarity of Stau2 and Ago1/2 when examining neuronal branching, indicating that this complex RBP network is important for neuronal function. Possibly this antagonistic action of both RBPs also results in the stabilization of mRNAs in Stau2 containing transport RNPs (5), that are translationally silenced by Ago proteins. Our data showing increased co-localization of Ago2 and Stau2 in distal dendrites, where directed transport of RNAs takes place, support this model. Here, a fine-tuned equilibrium of Stau2 and Ago proteins would ensure spatiotemporal control of translation that in turn critically contributes to neuronal function and synaptic plasticity. Together, our data suggest that Stau2 and Ago/RISC counterbalance each other on several levels, *e.g.* RNA stability, translation and neuronal morphology. It is by now well accepted that posttranscriptional gene expression is regulated at multiple levels in cells (3). Therefore, it does not come as a surprise that removing one defined layer may therefore disturb neuronal homeostasis yielding complex phenotypes in cells (2).

DATA AVAILABILITY

Small RNA sequencing data are available at the GEO database under the accession code GSE185935.

SUPPLEMENTARY DATA

Supplementary Data are available at NAR Online.

REFERENCES

1. Hentze,M.W., Castello,A., Schwarzl,T. and Preiss,T. (2018) A brave new world of RNA-binding proteins. *Nat. Rev. Mol. Cell Biol.*, **19**, 327–341.
2. Schieweck,R., Ninkovic,J. and Kiebler,M.A. (2021) RNA-binding proteins balance brain function in health and disease. *Physiol. Rev.*, **101**, 1309–1370.

3. Mata,J., Marguerat,S. and Bähler,J. (2005) Post-transcriptional control of gene expression: a genome-wide perspective. *Trends Biochem. Sci.*, **30**, 506–514.

4. Dassi,E. (2017) Handshakes and fights: the regulatory interplay of RNA-binding proteins. *Front. Mol. Biosci.*, **4**, 67.

5. Kiebler,M.A. and Bassell,G.J. (2006) Neuronal RNA granules: movers and makers. *Neuron*, **51**, 685–690.

6. Anderson,P. and Kedersha,N. (2006) RNA granules. *J. Cell Biol.*, **172**, 803–808.

7. Tauber,D., Tauber,G. and Parker,R. (2020) Mechanisms and regulation of RNA condensation in RNP granule formation. *Trends Biochem. Sci.*, **45**, 764–778.

8. Langdon,E.M., Qiu,Y., Ghanbari Niaki,A., McLaughlin,G.A., Weidmann,C.A., Gerbich,T.M., Smith,J.A., Crutchley,J.M., Termini,C.M., Weeks,K.M. *et al.* (2018) mRNA structure determines specificity of a polyQ-driven phase separation. *Science*, **360**, 922–927.

9. Mikl,M., Vendra,G. and Kiebler,M.A. (2011) Independent localization of MAP2, camkiiα and β-actin RNAs in low copy numbers. *EMBO Rep.*, **12**, 1077–1084.

10. Pilaz,L.-J., Lennox,A.L., Rouanet,J.P. and Silver,D.L. (2016) Dynamic mRNA transport and local translation in radial glial progenitors of the developing brain. *Curr. Biol.*, **26**, 3383–3392.

11. Hubstenberger,A., Courel,M., Bénard,M., Souquere,S., Ernoult-Lange,M., Chouaib,R., Yi,Z., Morlot,J.-B., Munier,A., Fradet,M. *et al.* (2017) P-Body purification reveals the condensation of repressed mRNA regulons. *Mol. Cell*, **68**, 144–157.

12. Sharangdhar,T., Sugimoto,Y., Heraud-Farlow,J., Fernández-Moya,S.M., Ehses,J., Ruiz de Los Mozos,I., Ule,J. and Kiebler,M.A. (2017) A retained intron in the 3′-UTR of calm3 mRNA mediates its Staufen2- and activity-dependent localization to neuronal dendrites. *EMBO Rep.*, **18**, 1762–1774.

13. Köhrmann,M., Luo,M., Kaether,C., Desgroseillers,L., Dotti,C.G. and Kiebler,M.A. (1999) Microtubule-dependent recruitment of staufen-green fluorescent protein into large RNA-containing granules and subsequent dendritic transport in living hippocampal neurons. *Mol. Biol. Cell*, **10**, 2945–2953.

14. Bauer,K.E., Segura,I., Gaspar,I., Scheuss,V., Illig,C., Ammer,G., Hutten,S., Basyuk,E., Fernández-Moya,S.M., Ehses,J. *et al.* (2019) Live cell imaging reveals 3′-UTR dependent mRNA sorting to synapses. *Nat. Commun.*, **10**, 3178.

15. Tang,S.J., Meulemans,D., Vazquez,L., Colaco,N. and Schuman,E. (2001) A role for a rat homolog of staufen in the transport of RNA to neuronal dendrites. *Neuron*, **32**, 463–475.

16. Heraud-Farlow,J.E., Sharangdhar,T., Li,X., Pfeifer,P., Tauber,S., Orozco,D., Hörmann,A., Thomas,S., Bakosova,A., Farlow,A.R. *et al.* (2013) Staufen2 regulates neuronal target RNAs. *Cell Rep.*, **5**, 1511–1518.

17. Goetze,B., Tuebing,F., Xie,Y., Dorostkar,M.M., Thomas,S., Pehl,U., Boehm,S., Macchi,P. and Kiebler,M.A. (2006) The brain-specific double-stranded RNA-binding protein staufen2 is required for dendritic spine morphogenesis. *J. Cell Biol.*, **172**, 221–231.

18. Lebeau,G., Miller,L.C., Tartas,M., McAdam,R., Laplante,I., Badeaux,F., DesGroseillers,L., Sossin,W.S. and Lacaille,J.-C. (2011) Staufen 2 regulates mGluR long-term depression and map1b mRNA distribution in hippocampal neurons. *Learn. Mem.*, **18**, 314–326.

19. Berger,S.M., Fernández-Lamo,I., Schönig,K., Fernández Moya,S.M., Ehses,J., Schieweck,R., Clementi,S., Enkel,T., Grothe,S., von Bohlen und Halbach,O. *et al.* (2017) Forebrain-specific, conditional silencing of staufen2 alters synaptic plasticity, learning, and memory in rats. *Genome Biol.*, **18**, 222.

20. Fritzsche,R., Karra,D., Bennett,K.L., Ang,F.yee, Heraud-Farlow,J.E., Tolino,M., Doyle,M., Bauer,K.E., Thomas,S., Planyavsky,M. *et al.* (2013) Interactome of two diverse RNA granules links mRNA localization to translational repression in neurons. *Cell Rep.*, **5**, 1749–1762.

21. Bartel,D.P. (2018) Metazoan MicroRNAs. *Cell*, **173**, 20–51.

22. Meister,G. (2013) Argonaute proteins: functional insights and emerging roles. *Nat. Rev. Genet.*, **14**, 447–459.

23. Jonas,S. and Izaurralde,E. (2015) Towards a molecular understanding of microRNA-mediated gene silencing. *Nat. Rev. Genet.*, **16**, 421–433.

24. Liu,J., Carmell,M.A., Rivas,F.V., Marsden,C.G., Thomson,J.M., Song,J.-J., Hammond,S.M., Joshua-Tor,L. and Hannon,G.J. (2004) Argonaute2 is the catalytic engine of mammalian RNAi. *Science*, **305**, 1437–1441.

25. Lessel,D., Zeitler,D.M., Reijnders,M.R.F., Kazantsev,A., Hassani Nia,F., Bartholomäus,A., Martens,V., Bruckmann,A., Graus,V., McConkie-Rosell,A. *et al.* (2020) Germline AGO2 mutations impair RNA interference and human neurological development. *Nat. Commun.*, **11**, 5797.

26. Nawalpuri,B., Ravindran,S. and Muddashetty,R.S. (2020) The role of dynamic miRISC during neuronal development. *Front. Mol. Biosci.*, **7**, 8.

27. Antoniou,A., Khudayberdiev,S., Idziak,A., Bicker,S., Jacob,R. and Schratt,G. (2018) The dynamic recruitment of TRBP to neuronal membranes mediates dendritogenesis during development. *EMBO Rep.*, **19**, e44853.

28. Zeitelhofer,M., Karra,D., Macchi,P., Tolino,M., Thomas,S., Schwarz,M., Kiebler,M. and Dahm,R. (2008) Dynamic interaction between P-Bodies and transport ribonucleoprotein particles in dendrites of mature hippocampal neurons. *J. Neurosci.*, **28**, 7555–7562.

29. Iadevaia,V. and Gerber,A.P. (2015) Combinatorial control of mRNA fates by RNA-Binding proteins and non-coding RNAs. *Biomolecules*, **5**, 2207–2222.

30. Quévillon Huberdeau,M., Zeitler,D.M., Hauptmann,J., Bruckmann,A., Fressigné,L., Danner,J., Piquet,S., Strieder,N., Engelmann,J.C., Jannot,G. *et al.* (2017) Phosphorylation of argonaute proteins affects mRNA binding and is essential for microRNA-guided gene silencing in vivo. *EMBO J.*, **36**, 2088–2106.

31. Braun,J., Misiak,D., Busch,B., Krohn,K. and Hüttelmaier,S. (2014) Rapid identification of regulatory microRNAs by miTRAP (miRNA trapping by RNA in vitro affinity purification). *Nucleic Acids Res.*, **42**, e66.

32. Heraud-Farlow,J.E. and Kiebler,M.A. (2014) The multifunctional staufen proteins: conserved roles from neurogenesis to synaptic plasticity. *Trends Neurosci.*, **37**, 470–479.

33. Vessey,J.P., Schoderboeck,L., Gingl,E., Luzi,E., Riefler,J., Di Leva,F., Karra,D., Thomas,S., Kiebler,M.A. and Macchi,P. (2010) Mammalian pumilio 2 regulates dendrite morphogenesis and synaptic function. *Proc. Natl. Acad. Sci. U.S.A.*, **107**, 3222–3227.

34. Ehses,J., Fernández-Moya,S.M., Schröger,L. and Kiebler,M.A. (2021) Synergistic regulation of rgs4 mRNA by HuR and miR-26/RISC in neurons. *RNA Biol.*, **18**, 988–998.

35. Zeitelhofer,M., Vessey,J.P., Xie,Y., Tübing,F., Thomas,S., Kiebler,M. and Dahm,R. (2007) High-efficiency transfection of mammalian neurons via nucleofection. *Nat. Protoc.*, **2**, 1692–1704.

36. Schieweck,R., Riedemann,T., Forné,I., Harner,M., Bauer,K.E., Rieger,D., Ang,F.yee, Hutten,S., Demleitner,A.F., Popper,B. *et al.* (2021) Pumilio2 and staufen2 selectively balance the synaptic proteome. *Cell Rep.*, **35**, 109279.

37. Wessel,D. and Flügge,U.I. (1984) A method for the quantitative recovery of protein in dilute solution in the presence of detergents and lipids. *Anal. Biochem.*, **138**, 141–143.

38. Mi,H., Muruganujan,A., Ebert,D., Huang,X. and Thomas,P.D. (2019) PANTHER version 14: more genomes, a new PANTHER GO-slim and improvements in enrichment analysis tools. *Nucleic Acids Res.*, **47**, D419–D426.

39. Szklarczyk,D., Gable,A.L., Lyon,D., Junge,A., Wyder,S., Huerta-Cepas,J., Simonovic,M., Doncheva,N.T., Morris,J.H., Bork,P. *et al.* (2019) STRING v11: protein–protein association networks with increased coverage, supporting functional discovery in genome-wide experimental datasets. *Nucleic Acids Res.*, **47**, D607–D613.

40. Mathys,H., Basquin,J., Ozgur,S., Czarnocki-Cieciura,M., Bonneau,F., Aartse,A., Dziembowski,A., Nowotny,M., Conti,E. and Filipowicz,W. (2014) Structural and biochemical insights to the role of the CCR4-NOT complex and DDX6 ATPase in MicroRNA repression. *Mol. Cell*, **54**, 751–765.

41. Yoon,J.-S., Mogilicherla,K., Gurusamy,D., Chen,X., Chereddy,S.C.R.R. and Palli,S.R. (2018) Double-stranded RNA binding protein, staufen, is required for the initiation of RNAi in coleopteran insects. *Proc. Natl. Acad. Sci. U.S.A.*, **115**, 8334–8339.

42. Macchi,P., Brownawell,A.M., Grunewald,B., DesGroseillers,L., Macara,I.G. and Kiebler,M.A. (2004) The Brain-specific Double-stranded RNA-binding protein staufen2. *J. Biol. Chem.*, **279**, 31440–31444.

43. Ren,Z., Veksler-Lublinsky,I., Morrissey,D. and Ambros,V. (2016) Staufen negatively modulates MicroRNA activity in caenorhabditis elegans. *G3 (Bethesda).*, **6**, 1227–1237.

44. Rajgor,D., Sanderson,T.M., Amici,M., Collingridge,G.L. and Hanley,J.G. (2018) NMDAR-dependent argonaute 2 phosphorylation regulates miRNA activity and dendritic spine plasticity. *EMBO J.*, **44**, 1–21.
45. Zeng,Y., Sankala,H., Zhang,X. and Graves,P.R. (2008) Phosphorylation of argonaute 2 at serine-387 facilitates its localization to processing bodies. *Biochem. J.*, **413**, 429–436.
46. Golden,R.J., Chen,B., Li,T., Braun,J., Manjunath,H., Chen,X., Wu,J., Schmid,V., Chang,T.-C., Kopp,F. *et al.* (2017) An argonaute phosphorylation cycle promotes microRNA-mediated silencing. *Nature*, **542**, 197–202.
47. Freimer,J.W., Hu,T.J. and Blelloch,R. (2018) Decoupling the impact of micrornas on translational repression versus RNA degradation in embryonic stem cells. *Elife*, **7**, e38014.
48. Horvathova,I., Voigt,F., Kotrys,A.V., Zhan,Y., Artus-Revel,C.G., Eglinger,J., Stadler,M.B., Giorgetti,L. and Chao,J.A. (2017) The dynamics of mRNA turnover revealed by single-molecule imaging in single cells. *Mol. Cell*, **68**, 615–625.
49. Höck,J., Weinmann,L., Ender,C., Rüdel,S., Kremmer,E., Raabe,M., Urlaub,H. and Meister,G. (2007) Proteomic and functional analysis of Argonaute-containing mRNA–protein complexes in human cells. *EMBO Rep.*, **8**, 1052–1060.
50. Nottrott,S., Simard,M.J. and Richter,J.D. (2006) Human let-7a miRNA blocks protein production on actively translating polyribosomes. *Nat. Struct. Mol. Biol.*, **13**, 1108–1114.
51. Vasudevan,S. and Steitz,J.A. (2007) AU-Rich-Element-Mediated upregulation of translation by FXR1 and argonaute 2. *Cell*, **128**, 1105–1118.
52. del Prete,M.J., Vernal,R., Dolznig,H., Müllner,E.W. and Garcia-Sanz,J.A. (2007) Isolation of polysome-bound mRNA from solid tissues amenable for RT-PCR and profiling experiments. *RNA*, **13**, 414–421.
53. Cougot,N., Babajko,S. and Séraphin,B. (2004) Cytoplasmic foci are sites of mRNA decay in human cells. *J. Cell Biol.*, **165**, 31–40.
54. Teixeira,D., Sheth,U., Valencia-Sanchez,M.A., Brengues,M. and Parker,R. (2005) Processing bodies require RNA for assembly and contain nontranslating mRNAs. RNA, **11**, 371–382.
55. Rocchi,A., Moretti,D., Lignani,G., Colombo,E., Scholz-Starke,J., Baldelli,P., Tkatch,T. and Benfenati,F. (2019) Neurite-Enriched microrna-218 stimulates translation of the glua2 subunit and increases excitatory synaptic strength. *Mol. Neurobiol.*, **56**, 5701–5714.
56. Schmidt,E.K., Clavarino,G., Ceppi,M. and Pierre,P. (2009) SUnSET, a nonradioactive method to monitor protein synthesis. *Nat. Methods*, **6**, 275–277.
57. Fernández-Moya,S.M., Ehses,J., Bauer,K.E., Schieweck,R., Chakrabarti,A.M., Lee,F.C.Y., Illig,C., Luscombe,N.M., Harner,M., Ule,J. *et al.* (2021) RGS4 RNA secondary structure mediates staufen2 RNP assembly in neurons. *Int. J. Mol. Sci.*, **22**, 13021.
58. Kim,H.H., Kuwano,Y., Srikantan,S., Lee,E.K., Martindale,J.L. and Gorospe,M. (2009) HuR recruits let-7/RISC to repress c-Myc expression. *Genes Dev.*, **23**, 1743–1748.
59. Sugimoto,Y., Vigilante,A., Darbo,E., Zirra,A., Militti,C., D'Ambrogio,A., Luscombe,N.M. and Ule,J. (2015) hiCLIP reveals the in vivo atlas of mRNA secondary structures recognized by staufen 1. *Nature*, **519**, 491–494.
60. Kedde,M., van Kouwenhove,M., Zwart,W., Oude Vrielink,J.A.F., Elkon,R. and Agami,R. (2010) A Pumilio-induced RNA structure switch in p27-3′ UTR controls miR-221 and miR-222 accessibility. *Nat. Cell Biol.*, **12**, 1014–1020.
61. Ruijtenberg,S., Sonneveld,S., Cui,T.J., Logister,I., de Steenwinkel,D., Xiao,Y., MacRae,I.J., Joo,C. and Tanenbaum,M.E. (2020) mRNA structural dynamics shape Argonaute-target interactions. *Nat. Struct. Mol. Biol.*, **27**, 790–801.
62. Micklem,D.R., Adams,J., Grünert,S. and St Johnston,D. (2000) Distinct roles of two conserved staufen domains in oskar mRNA localization and translation. *EMBO J.*, **19**, 1366–1377.